

EP/L014106/1  
**Supergen Wind Hub**  
Sustainable Power Generation and Supply  
- Wind Energy Technologies



Deliverable 5.1.1

**Report on Stress concentration estimation method for  
innovative blade design**

Delivered by:	<sup>1</sup> STFC Rutherford Appleton Laboratory		
Author(s):	Blanca Pascual <sup>1</sup>		
Delivery date:	31 <sup>st</sup> May 2017		
Distribution list:	Supergen Wind Consortium		
Version No	Status	Date	Checked by
1	Draft	31 <sup>st</sup> May 2017	T.Davenne and J.Halliday

Sponsored by



# 1 Introduction

The UK has a target of over 30% energy from renewables by 2020 to reduce its CO<sub>2</sub> emissions. For this, onshore and offshore wind have to increase their capacity, from 10.1GW and 5.3GW in May 2017, respectively to 13GW and 18GW by 2020. The SUPERGEN Wind Energy Technologies Consortium is a UK wind energy research consortium which was originally established by the EPSRC on 23rd March 2006 as part of its Sustainable Power Generation and Supply (SUPERGEN) programme. Its aim is to develop academic, industrial and policy linkages and to lead the technology strategy for driving forward UK wind energy research and for exploiting the research outcomes. This in turn should address the medium term challenges of scaling up to multiple wind farms, considering how to better build, operate and maintain multi-GW arrays of wind turbines whilst providing a reliable source of electricity whose characteristics can be effectively integrated into a modern power system such as that in the UK. The consortium is led by Strathclyde University, but also includes Durham, Loughborough, Cranfield, Manchester, Oxford, Surrey, Bristol, Imperial, Dundee and STFC, with expertise in wind turbine technology, aerodynamics, hydrodynamics, materials, electrical machinery, control, reliability and condition monitoring, and has the support of 18 industrial partners, including DNV GL and the Offshore Renewable Energy Catapult. Its activities were renewed in 2014, and is funded to 2019.

This report is related to work package 5.1, on innovative blade design for improved load control, where the use of sub-modelling is explored in ABAQUS to determine the extent to which this might improve the modelling and representation of the structural loads without adding unduly to processing time.

The operating lifetime of wind turbine blades is controlled by the fatigue properties of the composite materials they're made of. These materials are generally provided as fabrics (non-crimp fabrics, uniweave, woven), i.e. they have a 2D nature that is reconfigured into 3D shapes when the blade and its internal features (e.g. spars) are formed. Methods to assess fatigue life damage for 2D composites with in-plane loading have been the subject of several studies [3] but in regions such as the T-joint joining the blade spar to the aerodynamic profile, through thickness effects are non-negligible and 3D stress states have to be taken into account.

The initiation of damage in these regions can occur well before what would be expected in the base material subjected to in-plane loading. Numerical studies of these geometry-related fatigue issues are generally performed on test models of dimensions in the order of 0.1m [6, 10, 7], using a very fine solid elements mesh. Wind turbine blade FE models available for academic purposes have lengths two to three orders of magnitude larger than these T-joint test samples: e.g. the DTU 10MW turbine is 86.5m long [1]. These blade FE models use shell elements and including the fine mesh from the T-joint for an accurate stress assessment could be both computationally challenging and need a detailed knowledge of the geometry.

Here, a method is proposed to obtain a detailed description of the T-joint stresses, where a shell mesh size around the T-joints similar to the one described in DNV-RP-C203 [4], i.e. a size equal to the thickness ( $t$ ) of the shell, is used. A dummy blade subjected to gravity, centrifugal loading and aerodynamic loading from blade element momentum (BEM) is constructed to verify the method. Firstly, test cases are built using the same mesh/geometry, but different loading for each test case. Detailed stresses around the T-joint for the test cases are obtained using submodels. A vector of strains/stresses in the dummy blade around the T-joint are projected into a subspace made of similar vector from the shell models of the test cases. The coefficients of the decomposition can then be used to recompose the detailed stresses on the T-joint. Two test cases geometries and several vectors for the decomposition procedure are used in this report. The software abaqus has been used to carry out the FE analysis.

## 2 T-joint geometry

The T-joint geometry used here is the same as the one used in [10, 7], and its geometry and layup are described in Figure 1. Dimensions are in mm and this geometry has been modelled with a depth of 50mm.

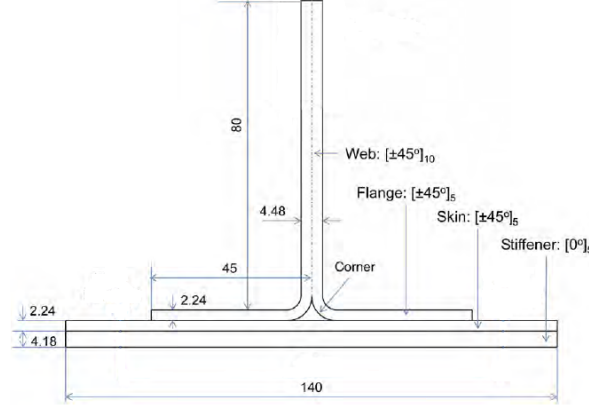
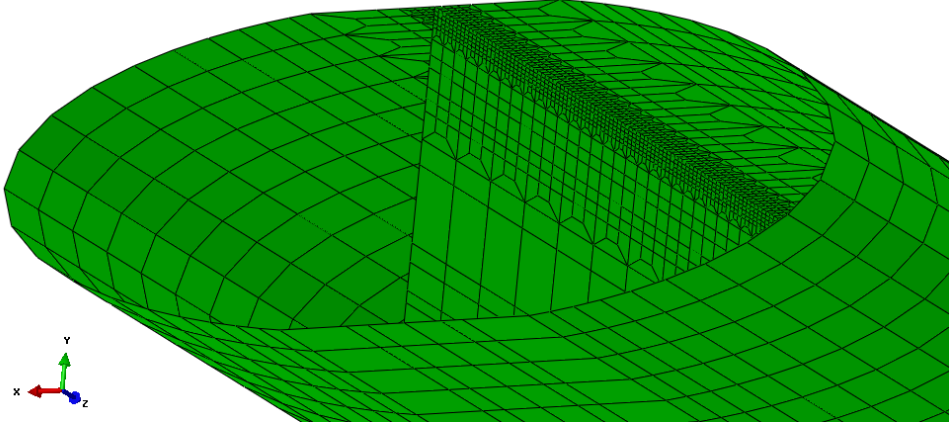


Figure 1: T-joint geometry

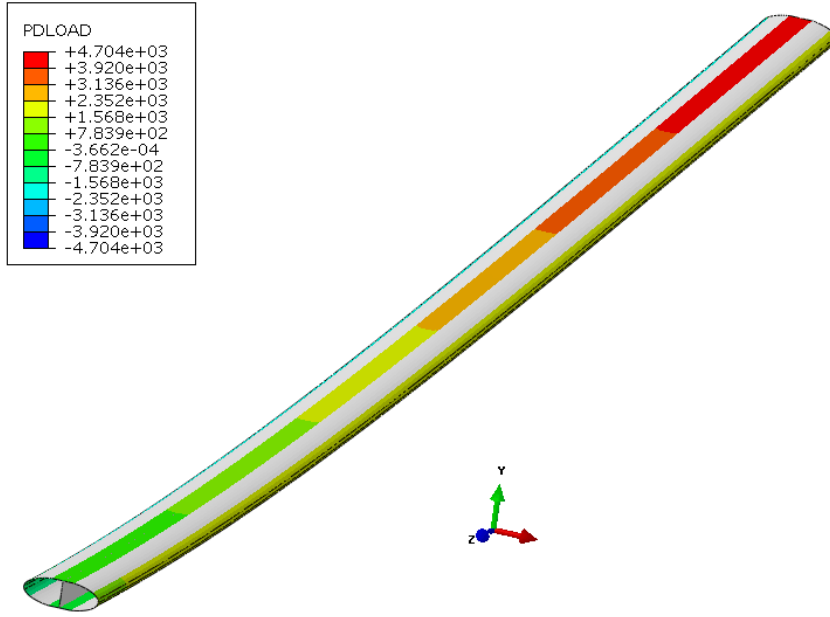
The T-joint is modelled using solid elements in the submodels, and using shells in the test cases and the blade dummy model. The orientation in all the models has been created such that the second axis corresponds to the direction of the fibre. The material properties of the uniaxial composite are: elastic moduli  $E1 = E3 = 9$  GPa,  $E2 = 38$  GPa; Poisson's ratios  $\nu_{13} = \nu_{23} = 0.3$ ,  $\nu_{12} = 0.071$ ; and the shear moduli  $G_{12} = G_{23} = 3.6$  GPa,  $G_{13} = 3.46$  GPa. Due to the elements orientation, stresses S11 are perpendicular to the fibre, S22 are in the direction of the fibre and S12 are shear stresses.

## 3 Blade element momentum loading on dummy blade

To verify the method (proposed in the next section), a dummy blade was created using S4R shell elements. This blade geometry is a simple extruded profile of length 25m, with the same layup at the T-joint as the one discussed in section 2, but the layup extends to create a profile. It is subjected to gravity, centrifugal load and pressures. The pressures are applied on four areas (top, bottom, leading edge, trailing edge), and on each area the pressure applied varies with Z (the distance to the root). The top and bottom pressures have the same norm but opposite value, so that both result in the same vertical force, the same happens with the leading edge/trailing edge pressures. The geometry of the profile with the mesh around the T-joint, and the surface variation in pressure with Z can be seen in Figure 2



(a) Long extruded profile mesh detail



(b) Long extruded profile pressure distribution

Figure 2: Geometry and aerodynamic loading of dummy blade

The section forces are obtained from basic rotor disc theory: it is assumed (for this dummy model check) that there are 3 blades. The forces in the Y direction (perpendicular to the rotor) and in the X direction (in the rotor plane, tangential to the blade) can be obtained from [2]

$$\mathbf{F}_y = 2\rho a(1-a)v_0^2 A/3 \quad \mathbf{F}_x = 2\rho(1-a)v_0 A\Omega a'R/3 \quad a = 1/3 \quad a' = \frac{a(1-a)}{\lambda R/R_{max}} \quad (1)$$

with  $\rho = 1.225 \text{ kg/m}^3$  the air density,  $v_0$  the wind speed,  $A$  the area of an annular ring of the actuator disc considered ( $A = \pi(R_e^2 - R_i^2)$ ),  $a = 1/3$  the the axial flow induction factor that maximizes the power coefficient when the turbine is modelled as an actuator disc (e.g. [2]),  $a'$  is the tangential flow induction factor,  $\Omega$  is the angular velocity,  $R$  the radius of the ring considered,  $R_{max}$  is the total radius of the rotor,  $\lambda = \Omega * R_{max}/v_0$  is the tip speed ratio. The blade is also subjected to centrifugal load ( $\Omega = 2.8 \text{ rad/s}$ ) and gravity load, with the gravity pointing in the -z direction, the root of the blade located at  $Z=0$ , and the tip at  $Z=-25\text{m}$ .

## 4 Proposed method

This work tries to extend the concept of hot spot method, e.g. in DNV-RP-C203 (developed for offshore steel structures), to composites. The code provides, in general, stress concentration factors for geometric details, and, in section 4, discusses fatigue for structures assessed using finite element analysis. It calculates the geometric stress concentration factor (SCF) with the FE model, and accounts for a notch factor resulting from the weld geometry/residual stresses, etc, that is included by using the appropriate S-N curves. In the code, the shells have a (recommended) mesh size of the thickness of the element ( $t$ ), resulting in square elements of size  $t$ , referred to as a  $t \times t$  mesh. The stress components parallel and perpendicular to the weld at the centroid of the two elements next to the weld (i.e. distances  $0.5t$  and  $1.5t$  from the weld) are obtained, and linearly extrapolated to the weld toe. This method could not be extrapolated to composites directly, as calculating stress concentration factors for two different loads lead to different results, and this first attempt used hot-spot stresses from a shell model, and detailed stresses from a submodel. Nonetheless, two ideas are used from the hot-spot method: the need to relate the stresses from a shell FE model to the ones in a geometrical detail, and the guidelines for mesh size around the T-joints.

There are two ways in which detailed stresses can be calculated at the T-joints: by directly including the fine mesh or using a submodel. Detailed stresses have been calculated on trailing edges of wind turbine blades by using directly a fine mesh in [5], but only a section of the blade was modelled, and continuum shell elements were used for positions which were a significant distance from the trailing edge, to reduce computational time. Alternatively, shell-to-solid ties could be used to include a solids mesh within a shell mesh. Here, a submodel of the T-joint is used, i.e. firstly analyzing the shell model of the blade and then imposing boundary conditions from this model into a solid elements model of the T-joint. Both methods would be computationally intensive if detailed stresses are needed for the whole T-joint of a 80-100m long blade, due to the small mesh size needed.

To avoid modelling directly the T-joints for the whole blade, here a more convoluted method is proposed, that should allow savings both in computational time and in pre-processing time due to using a simpler geometry.

The steps of the proposed method are as follow

- 1 Create test cases using shell elements. All the test cases use the same geometry but different loads.
- 2 Extract vectors of data  $\mathbf{v}$  for each of the test cases. These vectors are described in subsection 4.1.
- 3 Create solids submodels for the T-joint region of the test cases, so as to have a detailed representation of the stresses at the T-joint for the test cases
- 4 Create a matrix whose columns are the data vectors from the test cases, i.e.  $\mathbf{V} = [\mathbf{v}_1, \dots, \mathbf{v}_i]$ . Calculate its Moore-Penrose pseudo-inverse  $\mathbf{V}_{MP}^{-1}$
- 5 From the blade shell model subjected to aerodynamic, centrifugal, gravity, gyroscopic loading: obtain a vector of data  $\mathbf{v}_g$ , similar to the one from the test cases.
- 6 Pre-multiply the vector from 5 by the Moore-Penrose pseudo-inverse of 4. This results in a vector of coefficients  $\alpha = \mathbf{V}_{MP}^{-1} \mathbf{v}_g$ .
- 7 Combine the test cases submodels using the vector of coefficients  $\alpha$  from 6. This results in detailed stresses around the T-joint.

it is noted that steps 1 to 4 only need to be done once for a given T-joint geometry, while steps 5 to 7 can be carried out for each loading and location in the T-joint, as different vectors of coefficients  $\alpha$  will be obtained.

#### 4.1 Vectors of the Subspace Used in the Proposed Decomposition Method

Subspace decomposition is a popular method when reducing the size of a system. For example, when considering the FE model of a system affected by uncertainty, a Krylov subspace [9] and eigenvectors of the original system [8] amongst others, have been used. In these references, the reduction is applied to a system that uses directly the structure matrices. But here the T-joint mass and stiffness matrices are ignored, and the T-joint detailed stresses are assumed to depend on the data (e.g. strains and stresses) measured on a few shells, and these ones are rearranged into a vector. As several datum are measured, a vector basis with the same number of vectors as measured datum would allow for direct inversion of the matrix  $\mathbf{V}$  in step 6 in the method description. This approach has not been implemented because it would imply using the same number of test cases as there are datum, and defining these test cases representative of the loading within a beam is challenging. The subspace used instead is based on decomposing the blade shell results into the results of well-selected test cases. Several options in terms of data measured and test cases can be used.

Different types of data can be used; so that several basis for the subspace decomposition have been tried. The data used here have been extracted at the integration point of the shell elements next to the T-joint, located on the outer skin on both sides of the shear web, and on the shear web. As the elements have a size of the thickness ( $t$ ) of the shell they represent, the data has been extracted at distances from the T-joint of  $0.5t$ ,  $1.5t$ ,  $2.5t$ . Hot-spot stresses, i.e. extrapolations to the T-joint location using data from  $0.5t$  and  $1.5t$  locations, have also been used. The figure below highlights the elements where data has been extracted

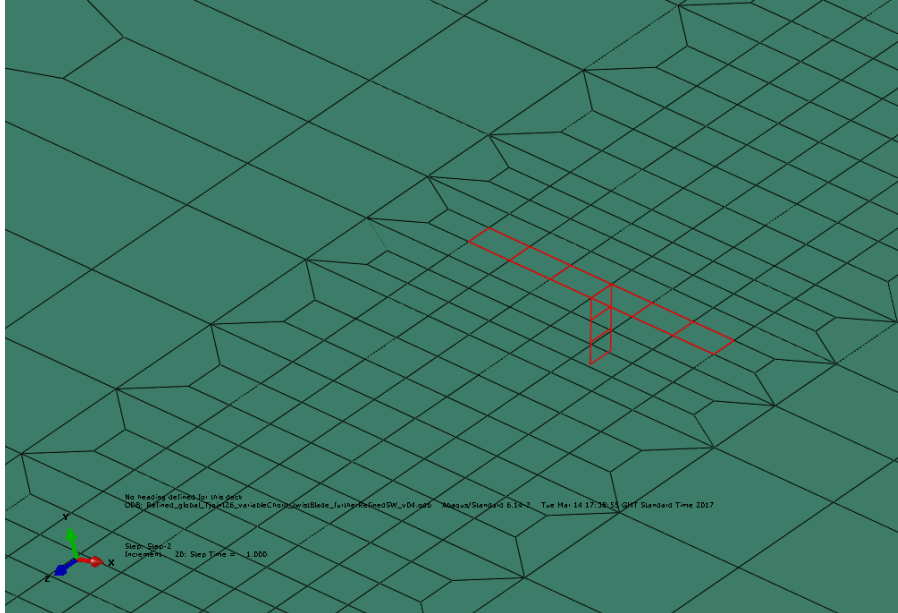


Figure 3: Elements around the T-joint where data is extracted

The vectors of data perused, so as to assess which ones works better, have been

Vector 1 Shell element membrane strains and curvatures in local 1 and 2 axis (outputs ‘SE1’, ‘SE2’, ‘SE3’, ‘SK1’, ‘SK2’, in abaqus) are extracted at  $0.5t$  and  $1.5t$ , i.e. for an element on

the outer skin and right side of the shear web, and at a distance 1.5t of the T-joint, a vector  $\mathbf{v}'_{OSR,1.5} = [SE1, SE2, SE3, SE3, SK1, SK2]$  is created. This leads to 5 (strains/curvatures) x 2 (distances from T-joint) x 3 (sides around the T-joint: outer skin right, outer skin left and shear web) = 30 datum to be used in each data vector of the test cases/global model, so that the data vector is given by

$$\mathbf{v} = \begin{bmatrix} \mathbf{v}_{OSR,0.5} \\ \mathbf{v}_{OSR,1.5} \\ \mathbf{v}_{OSL,0.5} \\ \mathbf{v}_{OSL,1.5} \\ \mathbf{v}_{SW,0.5} \\ \mathbf{v}_{SW,1.5} \end{bmatrix} \quad \text{with} \quad \mathbf{v}_{OSR,0.5} = \begin{bmatrix} SE1_{OSR,0.5} \\ SE2_{OSR,0.5} \\ SE3_{OSR,0.5} \\ SK1_{OSR,0.5} \\ SK2_{OSR,0.5} \end{bmatrix} \quad (2)$$

Vector 2 Shell element membrane strains and curvatures in local 1 and 2 axis extrapolated to the T-joint location (from 0.5t and 1.5t data), i.e. hot-spot strains and curvatures from shell elements. The data to be extracted is as in Vector 1, but the data vector is smaller (size 15) due to the hot-spot extrapolation.

$$\mathbf{v} = \begin{bmatrix} \mathbf{v}_{OSR,HS} \\ \mathbf{v}_{OSL,HS} \\ \mathbf{v}_{SW,HS} \end{bmatrix} \quad \text{with} \quad \mathbf{v}_{OSR,HS} = \begin{bmatrix} SE1_{OSR,HS} \\ SE2_{OSR,HS} \\ SE3_{OSR,HS} \\ SK1_{OSR,HS} \\ SK2_{OSR,HS} \end{bmatrix} \quad (3)$$

Vector 3 Shell element membrane stresses at the top and bottom of the shells ('S11', 'S22' and 'S12') extrapolated to the T-joint from values at 0.5t and 1.5t. This leads to 3 (stresses) x 2 (top/bottom shell location) x 2 (distances from T-joint) x 3 (shells around the T-joint) = 36 datum to be extracted, but the data vector is actually of size 18 as the hot-spot data (instead of 0.5t and 1.5t data) are used.

$$\mathbf{v} = \begin{bmatrix} \mathbf{v}_{OSR,top,HS} \\ \mathbf{v}_{OSR,bottom,HS} \\ \mathbf{v}_{OSL,top,HS} \\ \mathbf{v}_{OSL,bottom,HS} \\ \mathbf{v}_{SW,top,HS} \\ \mathbf{v}_{SW,bottom,HS} \end{bmatrix} \quad \text{with} \quad \mathbf{v}_{OSR,top,HS} = \begin{bmatrix} S11_{OSR,top,HS} \\ S22_{OSR,top,HS} \\ S12_{OSR,top,HS} \end{bmatrix} \quad (4)$$

Vector 4 Shell membrane strains at the top and bottom of the shells ('E11', 'E22' and 'E12' outputs in abaqus for the topmost and bottommost section points of the shells) at distances 0.5t and 1.5t of the T-joint. This leads to 3 (strains) x 2 (top/bottom shell location) x 2 (distances from T-joint) x 3 (shells around the T-joint) = 36 datum to be used in each data vector of the test cases/global model.

$$\mathbf{v} = \begin{bmatrix} \mathbf{v}_{OSR,top} \\ \mathbf{v}_{OSR,bottom} \\ \mathbf{v}_{OSL,top} \\ \mathbf{v}_{OSL,bottom} \\ \mathbf{v}_{SW,top} \\ \mathbf{v}_{SW,bottom} \end{bmatrix} \quad \text{with} \quad \mathbf{v}_{OSR,top} = \begin{bmatrix} E11_{OSR,top,0.5t} \\ E22_{OSR,top,0.5t} \\ E12_{OSR,top,0.5t} \\ E11_{OSR,top,1.5t} \\ E22_{OSR,top,1.5t} \\ E12_{OSR,top,1.5t} \end{bmatrix} \quad (5)$$

Vector 5 Shell membrane strains at the top and bottom of the shells extrapolated to the T-joint location (from strains at 0.5t and 1.5t). The data vector has a size of 3x2x1x3=18

$$\mathbf{v} = \begin{bmatrix} \mathbf{v}_{OSR,top} \\ \mathbf{v}_{OSR,bottom} \\ \mathbf{v}_{OSL,top} \\ \mathbf{v}_{OSR,bottom} \\ \mathbf{v}_{SW,top} \\ \mathbf{v}_{SW,bottom} \end{bmatrix} \quad \text{with} \quad \mathbf{v}_{OSR,top} = \begin{bmatrix} E11_{OSR,top,HS} \\ E22_{OSR,top,HS} \\ E12_{OSR,top,HS} \end{bmatrix} \quad (6)$$

Vector 6 Shell membrane strains at the top and bottom of the shells at distances 0.5t, 1.5t and 2.5t from the T-joint. The data vector has a size of 3x2x3x3=54

$$\mathbf{v} = \begin{bmatrix} \mathbf{v}_{OSR,top} \\ \mathbf{v}_{OSR,bottom} \\ \mathbf{v}_{OSL,top} \\ \mathbf{v}_{OSR,bottom} \\ \mathbf{v}_{SW,top} \\ \mathbf{v}_{SW,bottom} \end{bmatrix} \quad \text{with} \quad \mathbf{v}_{OSR,top} = \begin{bmatrix} E11_{OSR,top,0.5t} \\ E22_{OSR,top,0.5t} \\ E12_{OSR,top,0.5t} \\ E11_{OSR,top,1.5t} \\ E22_{OSR,top,1.5t} \\ E12_{OSR,top,1.5t} \\ E11_{OSR,top,2.5t} \\ E22_{OSR,top,2.5t} \\ E12_{OSR,top,2.5t} \end{bmatrix} \quad (7)$$

## 5 Test models

The viability of two different geometries for the test cases is assessed, by creating different test cases for each geometry. The first geometry consists of using a shell model with the same geometry as the submodel (coupon geometry) and its test cases are discussed in subsection 5.2, while the second is a simplified version of a blade section with longer chord than out-of-plan length and is discussed in subsection 5.3. Each test case of each geometry has been subjected to different boundary conditions (BCs) and loading. It is noted that, although a blade should be analyzed using the nonlinear geometry capabilities of abaqus, the aim of the test cases is to recreate the BCs of the submodel through a linear superposition of test cases using the coefficients from  $\alpha$ , and it is assumed that the geometrical nonlinearities within the submodel are negligible.

### 5.1 Submodel

The same submodel geometry (nodes, elements) is run with each test model of both subsections 5.2 and 5.3, and also with the dummy blade, so that the only variation between submodel runs are the global model used, the steps definition (so as to match those of the global model), and the location/angle where it is instanced. The layup and geometry is as defined in Section 2. The mesh, see Figure 4, uses fully integrated solid elements. Initial models used continuum shell elements and hourglassing problems were observed. As using the maximum hourglass stiffness allowed by abaqus did not solve the hourglass problem, fully integrated continuum shell elements are not available in abaqus and the aspect ratio of the elements allowed to use solid elements instead of continuum shells, they were swapped to fully integrated first order solid elements.

In Figure 4, the elements where stresses are extracted to obtain detailed stresses in Step 3 of section 4 are highlighted, and several distances across the path where those stresses are extracted are provided. For all the plies in the shear web, the distance across the radius of the



bend is scaled so that they have the same total distance, and this distance matches the one used for the shell elements in section 6.

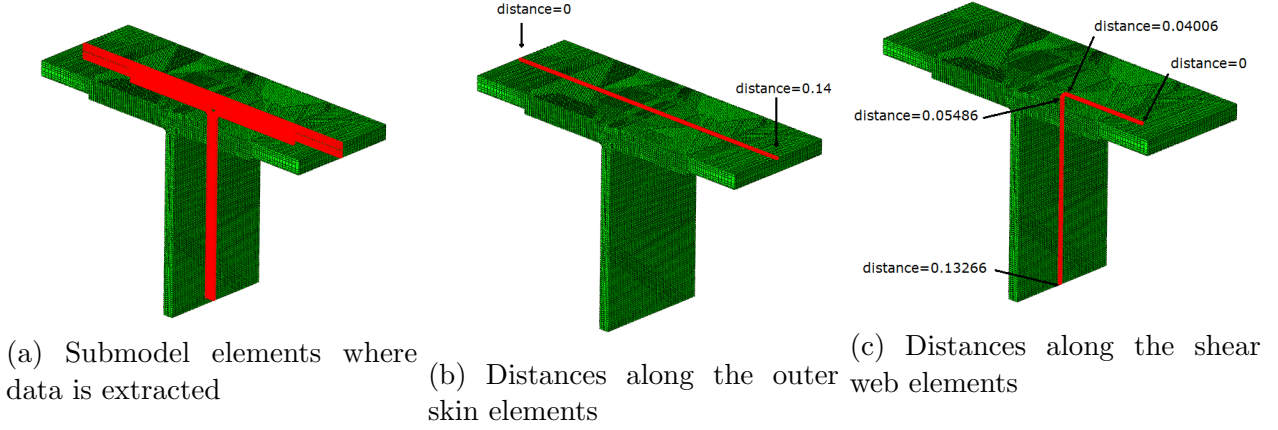


Figure 4: Submodel elements where stresses are extracted, and distances used to plot the results

## 5.2 Coupon test models

The coupon geometry/layup is as in Section 2, with a depth of 5cm, and the FE model mesh is displayed below, with the different nodes where boundary conditions are applied highlighted in red. It is noted that equations linking corresponding nodes on the two T sides of the T-joint have been defined, so that the difference in displacements and rotations between the two nodes is equal to the displacement/rotation of a dummy node.

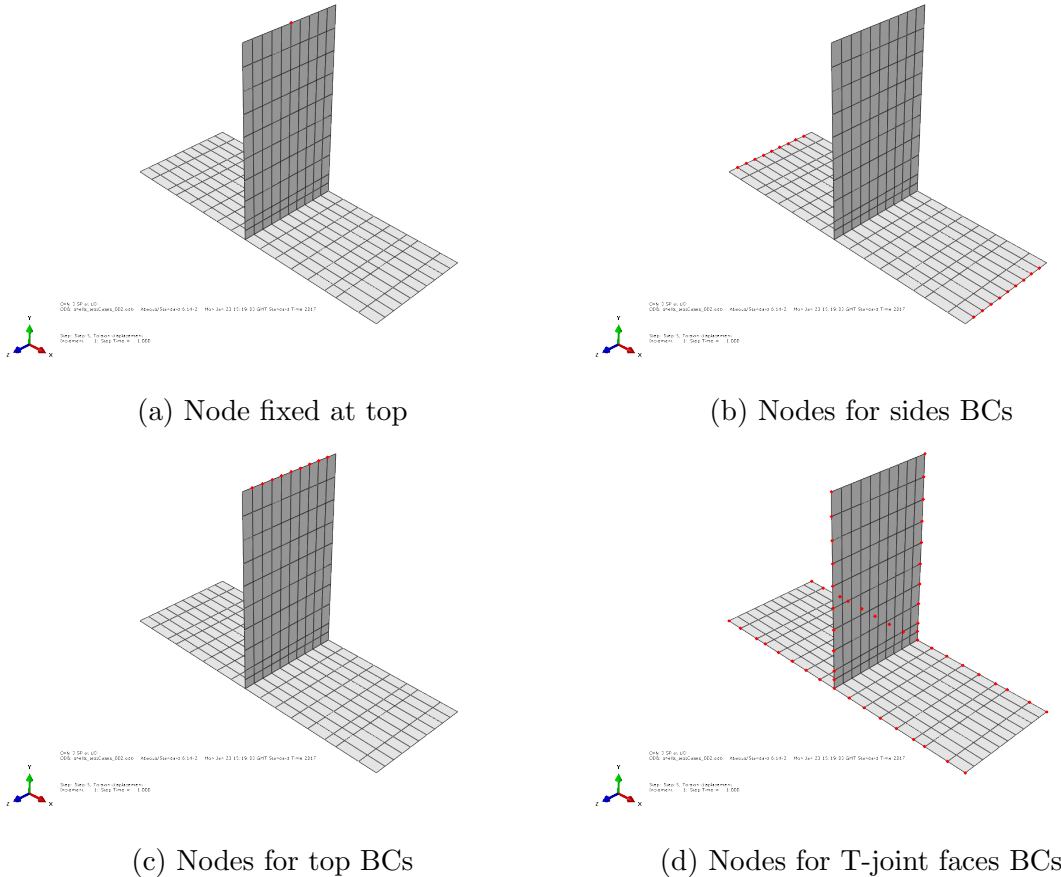


Figure 5: Nodes and elements where BCs/loads are applied to the T-joint tests mesh

In Figure 5, the T-joint is a T in the x-y plane, with the shear web pointing upwards in the direction of axis y. The test cases using this geometry are:

1. Pull-out: the node from Figure 5a is fixed in x, z and rotation around z ( $R_z$ ), the nodes on Figure 5b are fixed in y and  $R_z$ , the nodes in Figure 5c are displaced 0.001m in y and fixed in x and  $R_z$ . The dummy nodes have zero displacement/rotation (i.e the corresponding nodes on the front and rear faces have same displacements/rotations).
2. Tension: the node from Figure 5a is fixed in x, z and  $R_z$ , the nodes on Figure 5b are fixed in  $R_z$ , the nodes in Figure 5c are fixed in  $R_z$ . The dummy nodes have a displacement of 0.001m in z, and their remaining degrees of freedom (dofs) are fixed.
3. Rotation around X axis: the node from Figure 5a is fixed in x, y, z and  $R_z$ , the nodes on Figure 5b are fixed in  $R_z$ , the nodes in CouponShellYmax are fixed in  $R_z$ . The dummy nodes have a displacement in z that varies linearly with their Y location, and their remaining dofs are fixed.
4. Rotation around Y axis: the node from Figure 5a is fixed in x, y, z and  $R_z$ , the nodes on Figure 5b are fixed in  $R_z$ , the nodes in Figure 5c are fixed in  $R_z$ . The dummy nodes have a displacement in z that varies linearly with their Y location, and their remaining dofs are fixed.
5. Torsion: the node from Figure 5a is fixed in x, y, z and  $R_z$ , the nodes on Figure 5b are fixed in  $R_y$ ,  $R_z$ , and z; the nodes in Figure 5c are fixed in  $R_z$ . The dummy nodes have a displacement in x of 0.001m (the two T-joint faces are separated in x, so that the model is sheared), but other dofs are equal on corresponding nodes. The nodes on one of the faces are fixed in Z,  $R_x$  and  $R_y$  (so that they are also fixed on the other face).

These displacements are displayed below (multiplied by a scale factor auto-computed by abaqus)

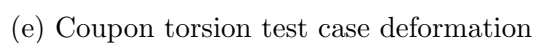
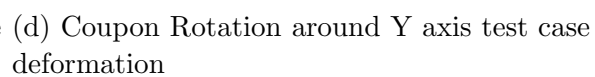
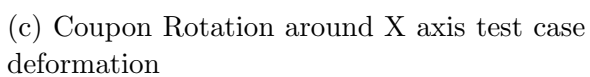
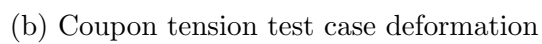
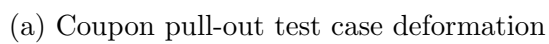
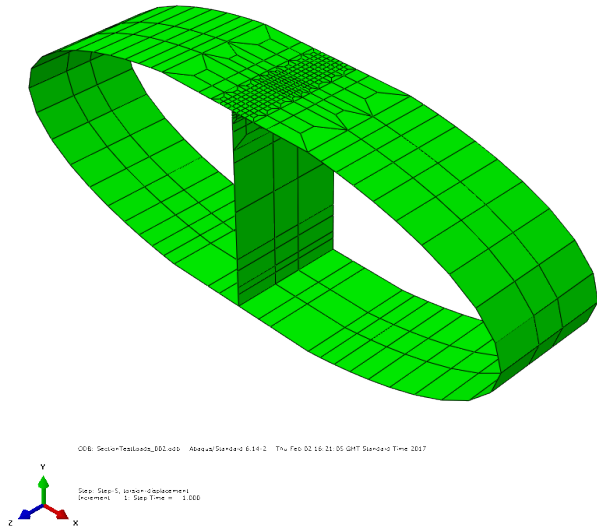


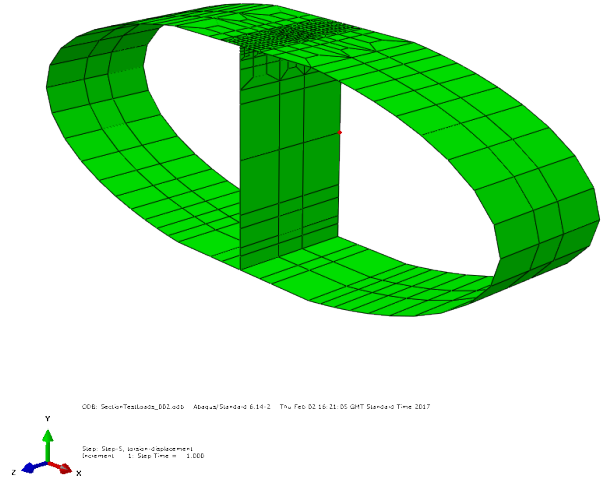
Figure 6: Test cases magnitude of displacement for the T-joint geometry

### 5.3 Blade section test models

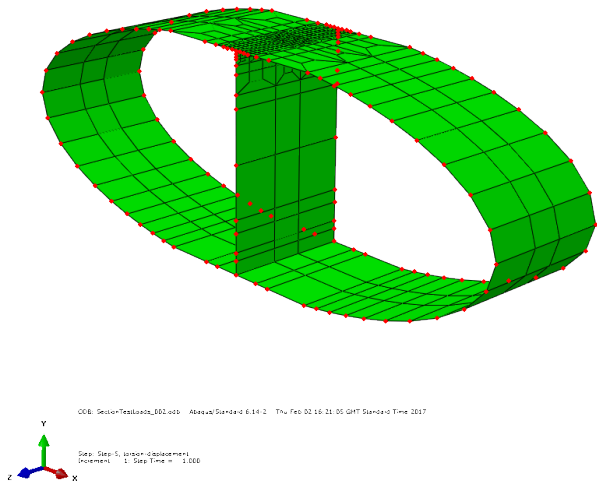
When the method was applied using the coupon test model discussed in subsection 5.2, the combination of stresses from the test cases did not match the results from the dummy blade. These poor results will be discussed in subsection 6.1. The blade section test model was developed to address this issue. The geometry of this test model has the same layup at the T-joint as the coupon, but the layup extends to create a profile, so that the boundary conditions on the top and sides of the T-joint are closer to reality. The profile and mesh are given in Figure 7a, together with the nodes and elements that have BCs/loads applied to them in the test cases. These test models also use equations linking the corresponding nodes of the two sides of the blade section highlighted in Figure 7c. Each of these equations includes a term depending on a dummy node, so as to specify the difference in displacement between the two mesh nodes affected by the equation.



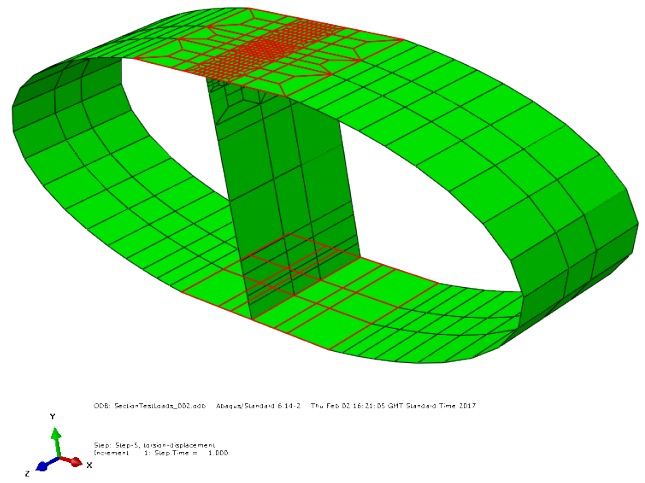
(a) Blade section test case geometry



(b) Blade section test fixed node



(c) Blade section nodes used in equations



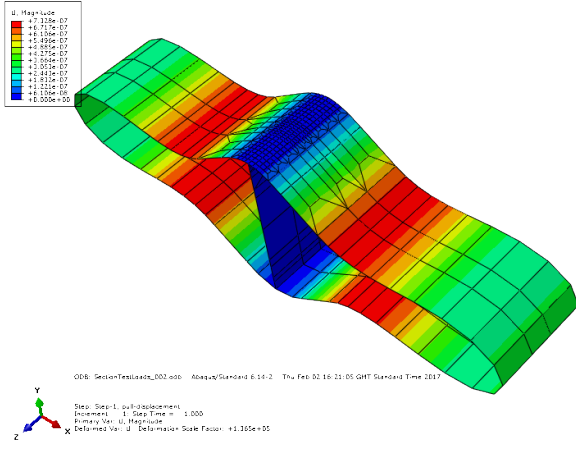
(d) Blade section elements where pressure is applied

Figure 7: Nodes and elements where BCs/loads are applied to the blade section tests mesh

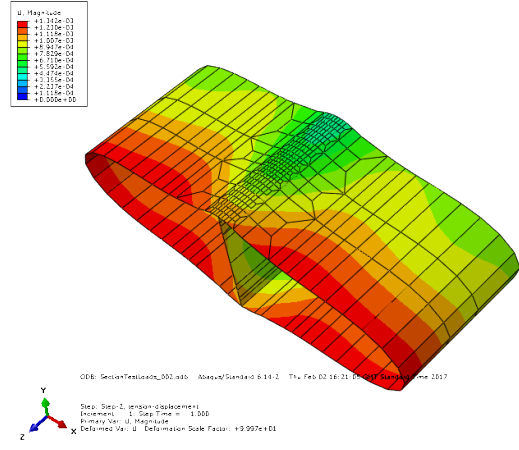
The test cases used with this geometry are

1. Pull-out: the node from Figure 7b is fixed in all dofs, the equations dummy nodes are fixed in all dofs, i.e. the corresponding nodes on Figure 7c have the same displacement/rotation. A pressure of 10Pa is applied on the surfaces from Figure 7d.
2. Tension: the node from Figure 7b is fixed in all dofs. The equations' dummy nodes have a displacement of 0.001 in z, and their remaining dofs are fixed.
3. Rotation around X axis: the node from Figure 7b is fixed in x, y, z and Rz. The dummy nodes have a displacement in z that varies linearly with their Y location, and their displacements in x and y, and rotations Ry, Rz are fixed.
4. Rotation around Y axis: the node from Figure 7b is fixed in x, y, z and Rz. The dummy nodes have a displacement in z that varies linearly with their Y location, and their displacements in x and y, and rotations Rx, Rz are fixed.
5. Torsion: the node from Figure 7b is fixed in x, y, z and Rz. The dummy have a displacement in x and y proportional to the centre of the section (x and y equal to 0), leading to a rotation of 1.146 degrees of the front face with respect to the back face.

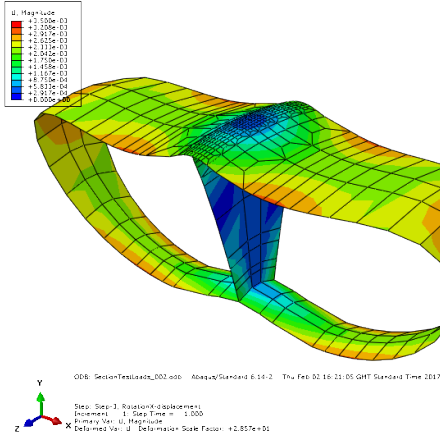
These displacements are displayed below (multiplied by a scale factor auto-computed by abaqus)



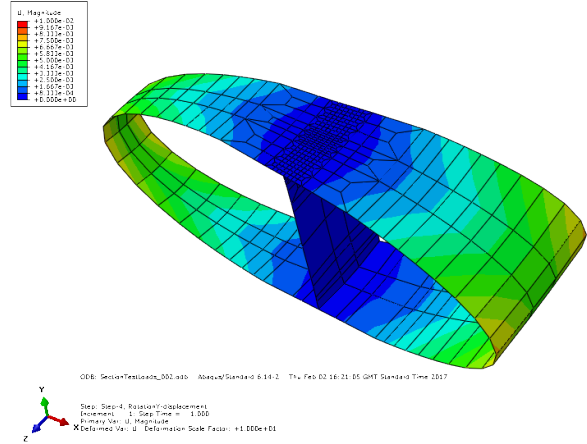
(a) Coupon pull-out test case deformation



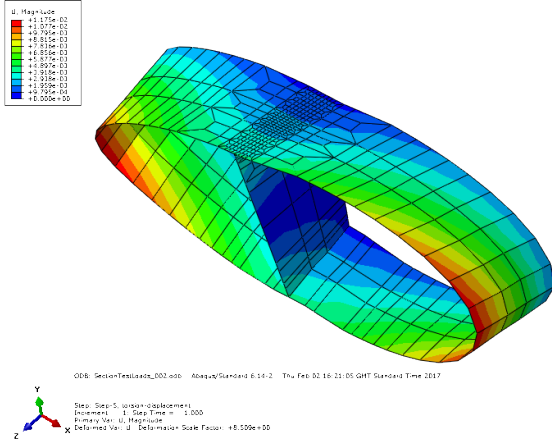
(b) Coupon tension test case deformation



(c) Coupon Rotation around X axis test case deformation



(d) Coupon Rotation around Y axis test case deformation



(e) Coupon torsion test case deformation

Figure 8: Test cases magnitude of displacement for the blade section tests mesh

## 6 Results

All the test cases are run as linear analyses. Scripts extracting results of stresses (S11, S22, S12) for each ply represented of the T-joint at the central section of the submodel have been created. These scripts can obtain stress results from the dummy blade, both from the shells

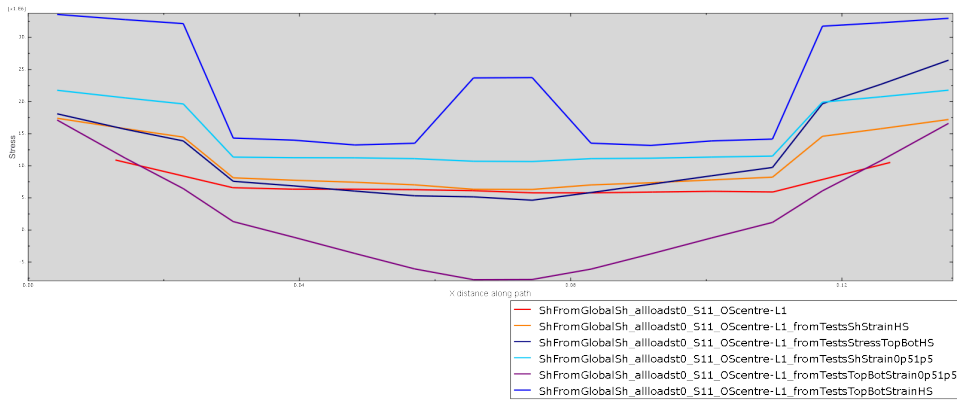
and the submodels. They can also apply Step 7 in subsection 4 to stresses from test cases using shell elements (i.e. the test cases global model) and using solid elements (i.e. the submodels of these global models). Here, only the shell stresses obtained from the dummy blade and the ones obtained from combining tests cases global models are displayed in subsections 6.1 and 6.2.

As a sanity check, it was verified that  $\mathbf{v}_i - \mathbf{V}_{MP}^{-1}\mathbf{v}_i$  is zero for each  $\mathbf{v}_i$  obtained in Step 2 of section 4.

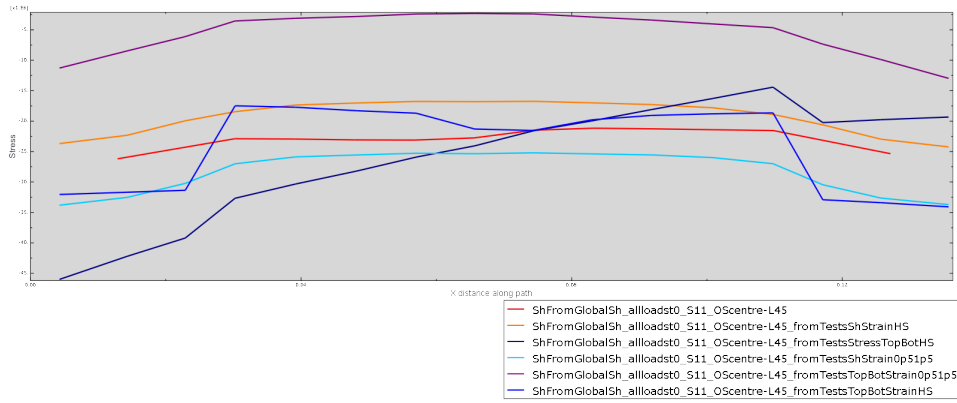
Unfortunately, results from the two test cases attempted were not very accurate, as can be seen in the Figures of subsections 6.1 and 6.2.

## 6.1 T-joint test cases

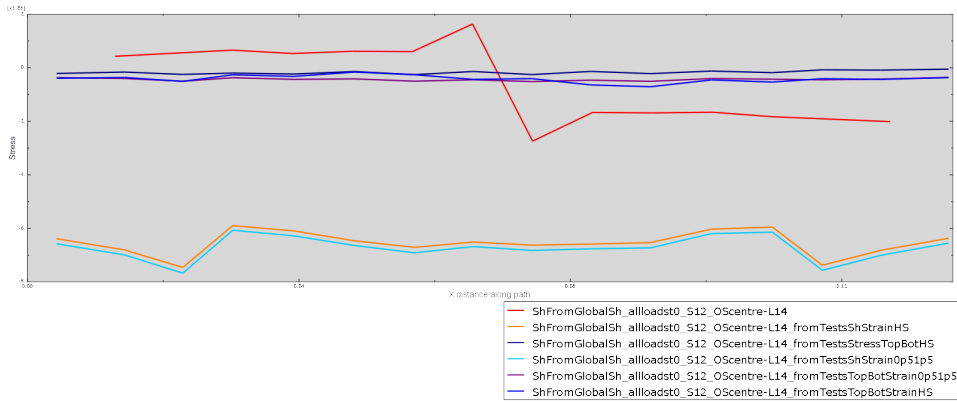
Results are plotted for some stresses of some plies, indicated in the caption of each subfigure in figures 9, 10, 11 and 12. The comparison is only performed for shell results, i.e. stresses on the blade model and in the linear combination of shell test cases. It is clear from the lack of agreement that the geometry is not suitable for the method developed.



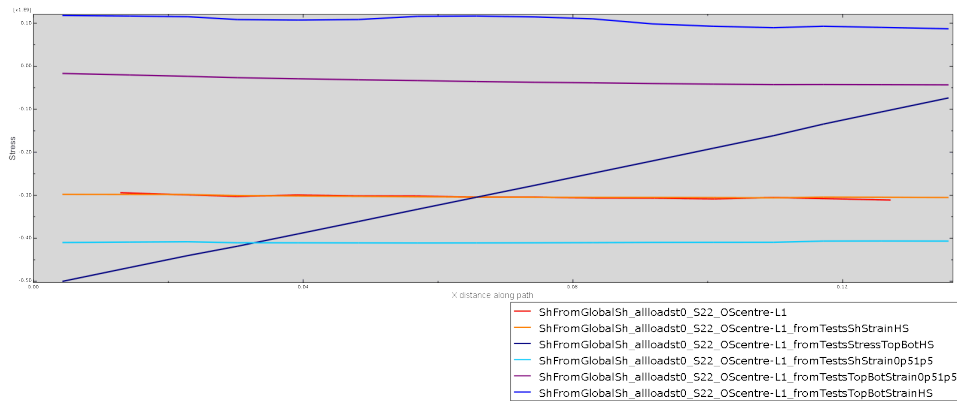
(a) S11, Outer Skin Bottom of ply-1



(b) S11, Outer Skin Top of ply-15



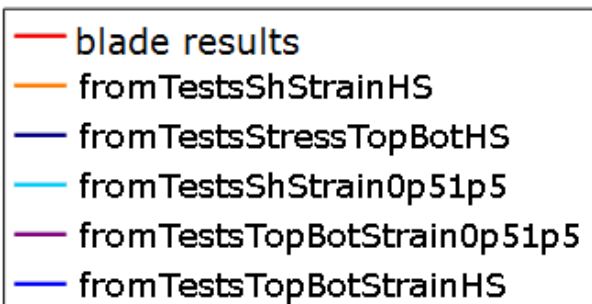
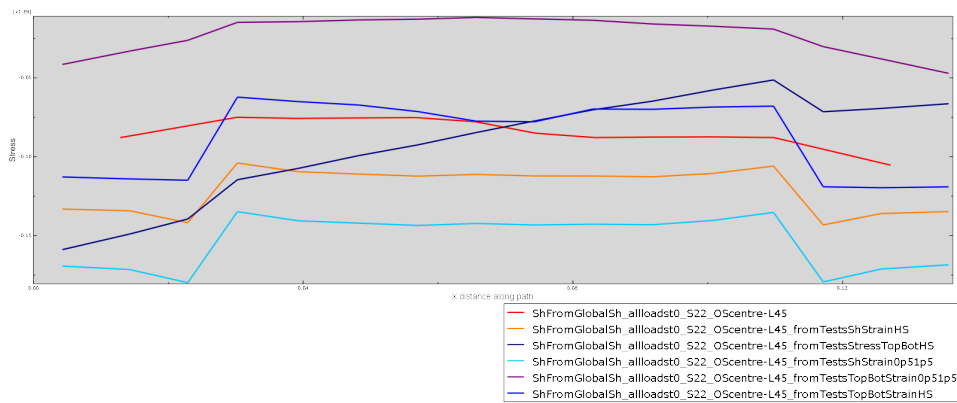
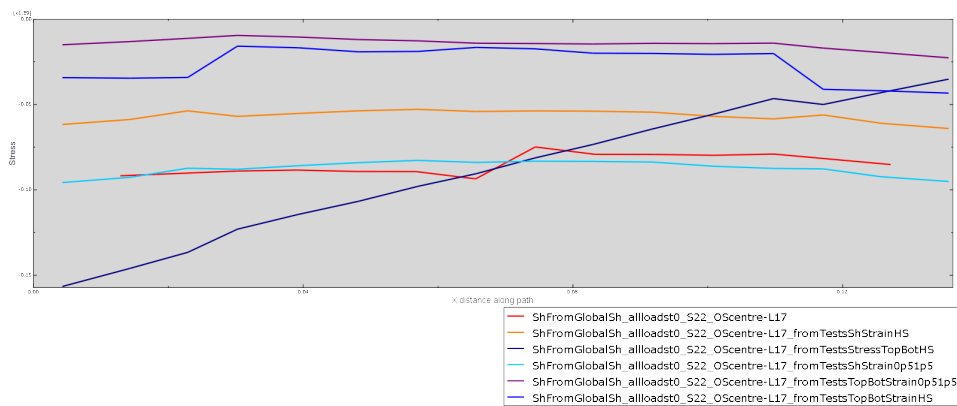
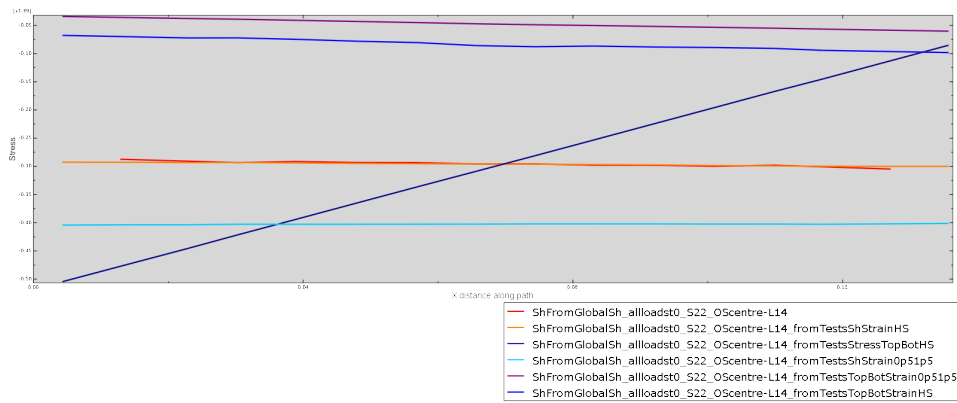
(c) S12, Outer Skin middle section point of ply-5 (UD ply)



(d) S22, Outer Skin Bottom of ply-1

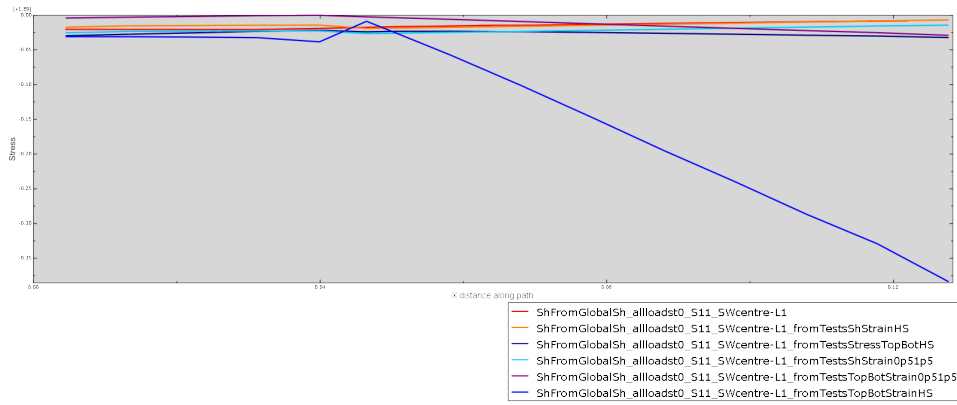
Figure 9: Coupon test cases stress results for the outer skin



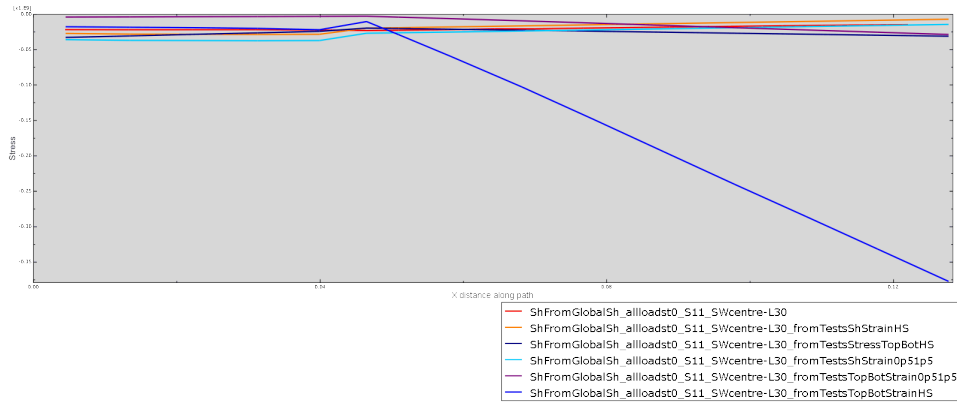


(d) Legend

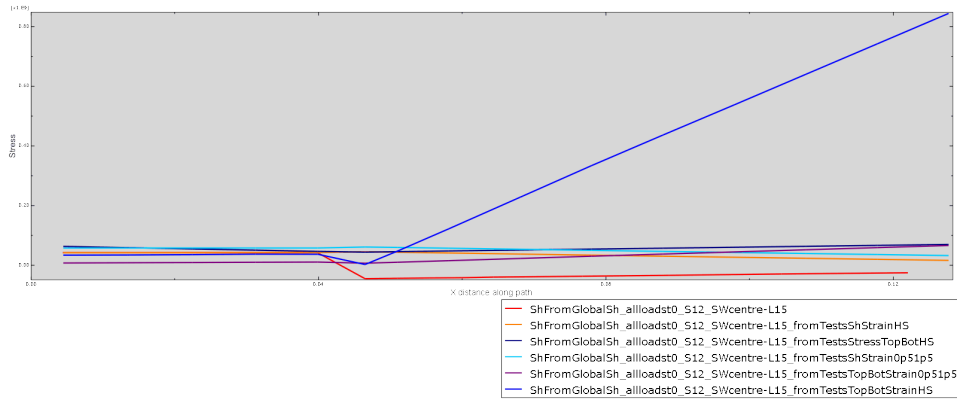
Figure 10: Coupon test cases stress results for the outer skin



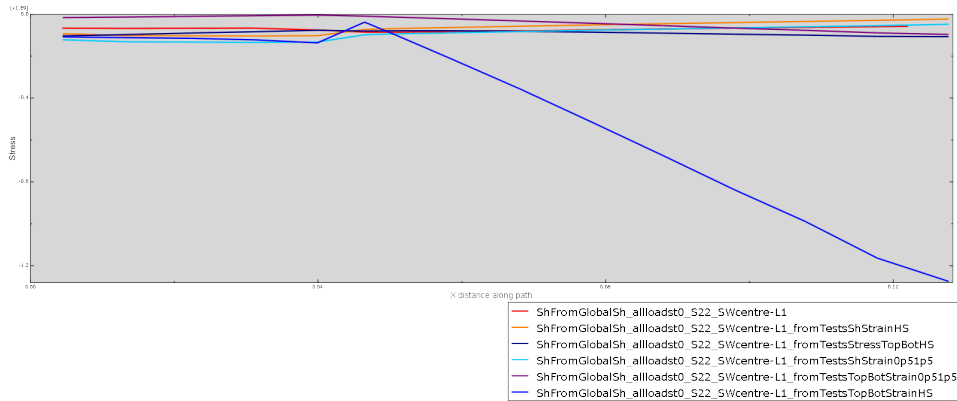
(a) S11, Shear Web Bottom of ply-1 (on the surface of the SW)



(b) S11, Shear Web last section point of ply-15 (-45, in contact with OS ply)

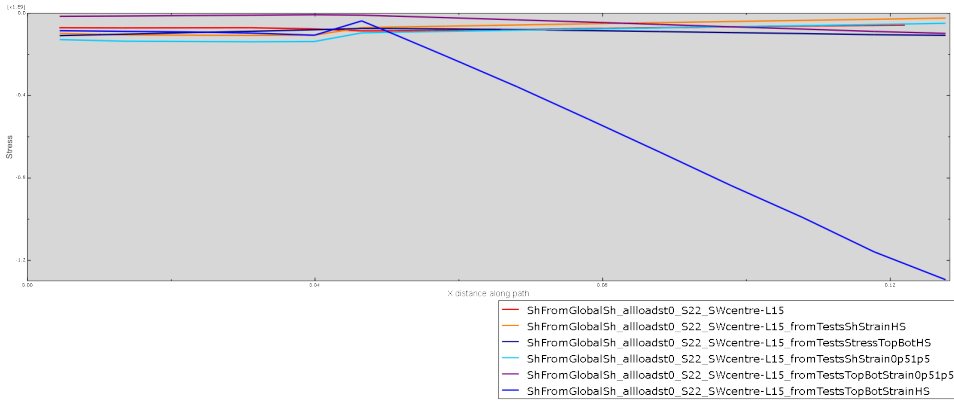


(c) S12, Shear Web ply-5

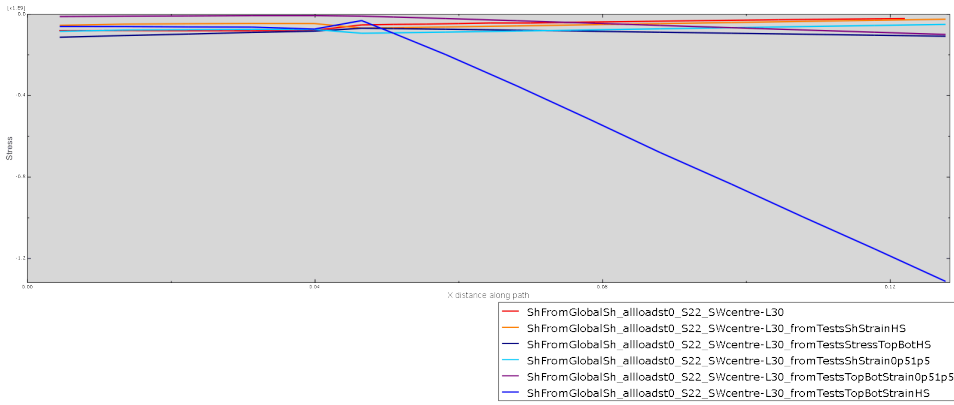


(d) S22, Shear Web Bottom of ply-1 (on the surface of the SW)

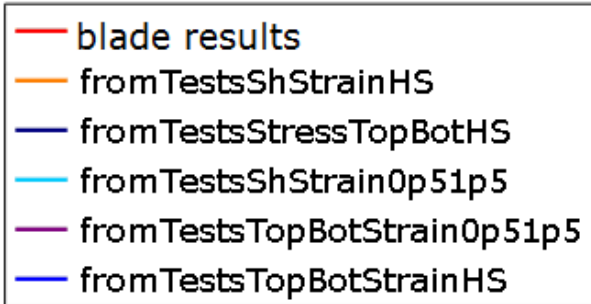
Figure 11: Coupon test cases stress results for the shear web



(a) S22, Shear Web ply-5



(b) S22, Shear Web ply-10

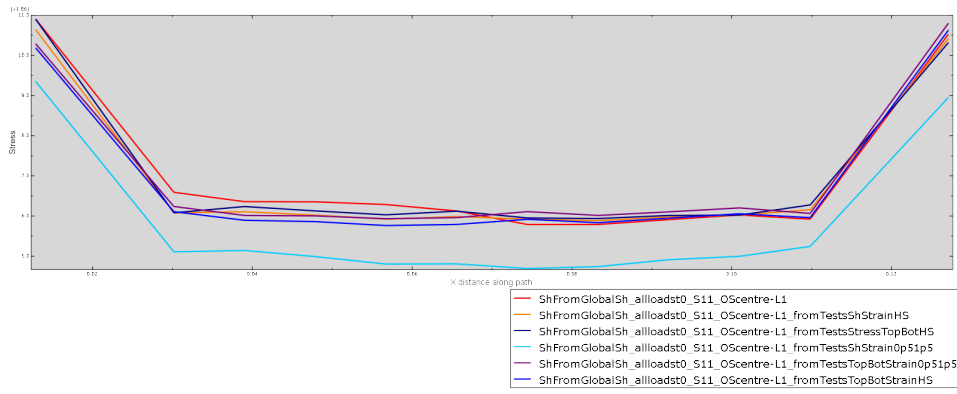


(c) Legend

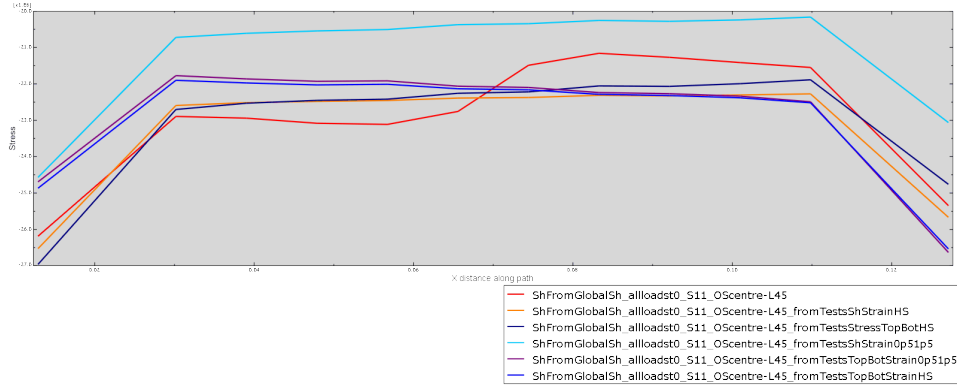
Figure 12: Coupon test cases stress results for the shear web

## 6.2 Blade section test cases

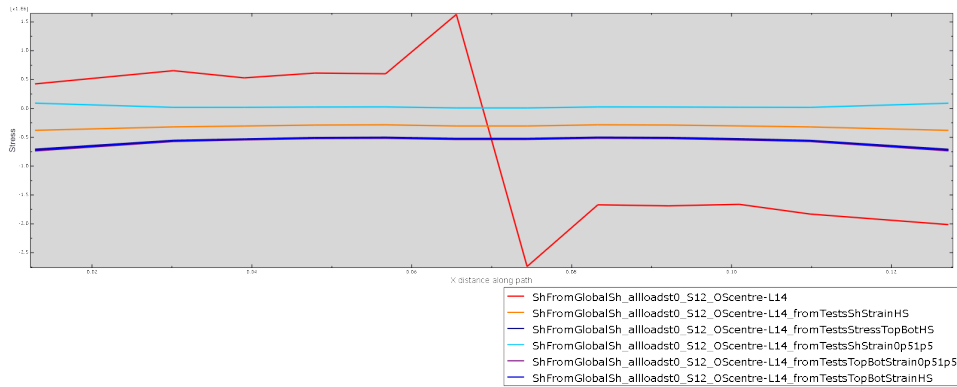
As for the previous test cases geometry, results are plotted in figures 13, 14, 15 and 16 for some stresses of some plies, indicated in the caption of each subfigure, and the comparison is only performed for shell results. It is clear from the lack of agreement that the geometry is not suitable for the method developed.



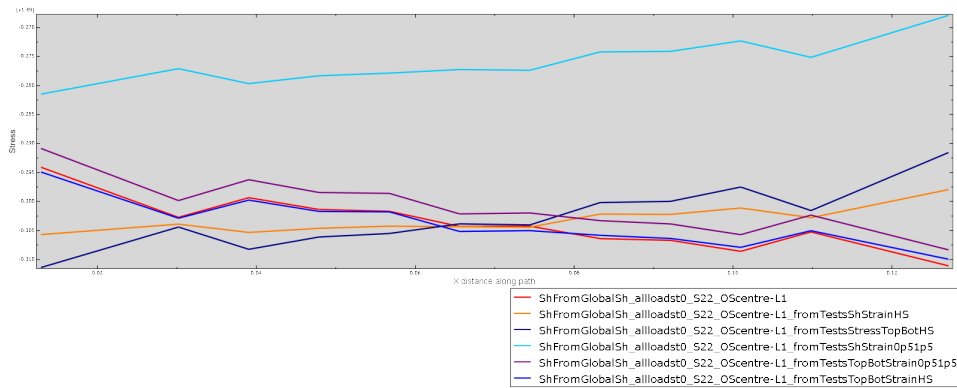
(a) S11, Outer Skin Bottom of ply-1



(b) S11, Outer Skin Top of ply-15

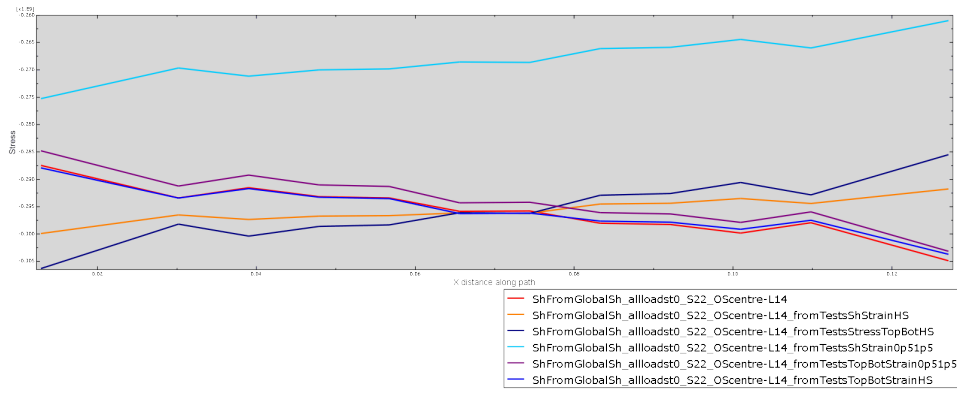


(c) S12, Outer Skin middle section point of ply-5 (UD ply)

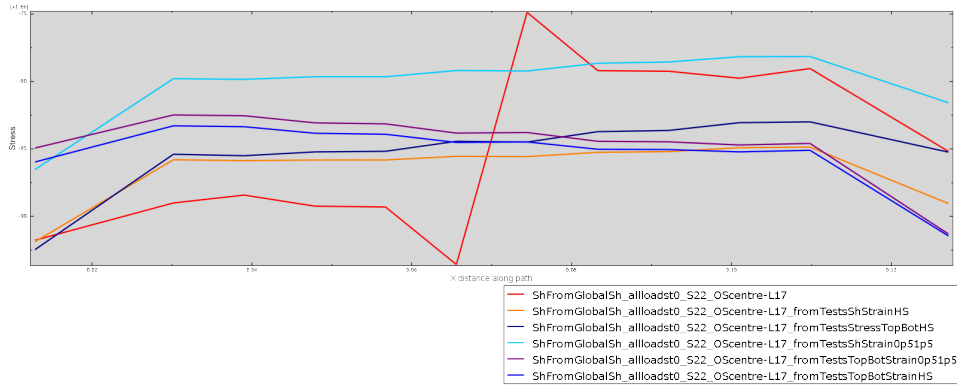


(d) S22, Outer Skin Bottom of ply-1

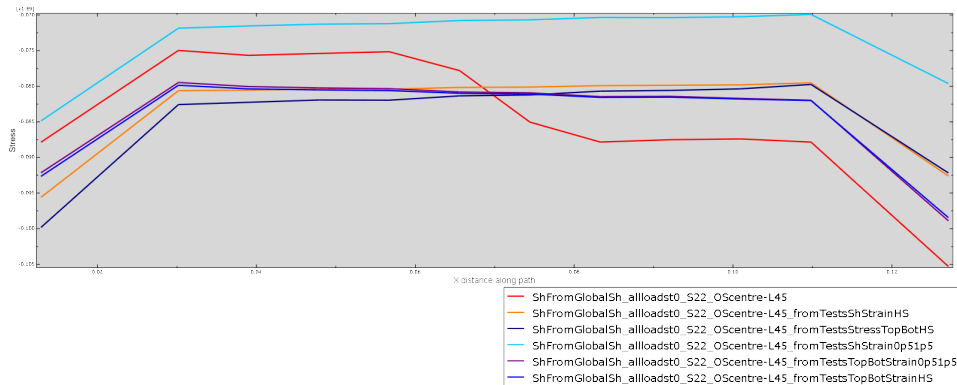
Figure 13: Blade section test cases stress results for the outer skin



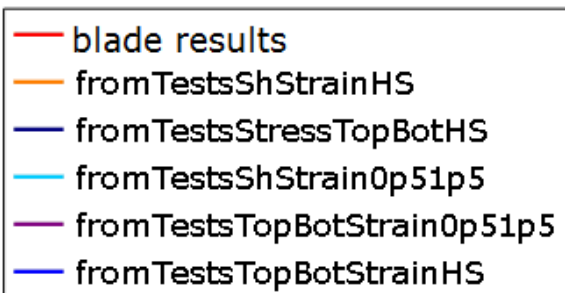
(a) S22, Outer Skin middle section point of ply-5 (UD ply)



(b) S22, Outer Skin middle section point of ply-6 (first -45 ply)

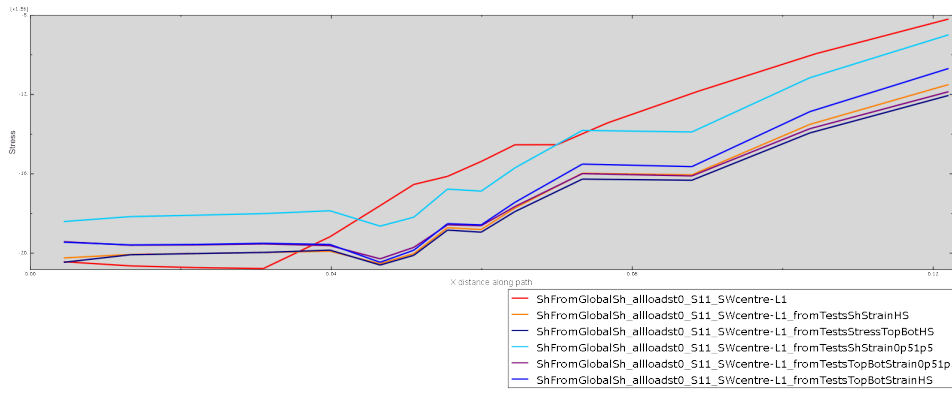


(c) S22, Outer Skin middle section point of ply-15 (last 45 ply)

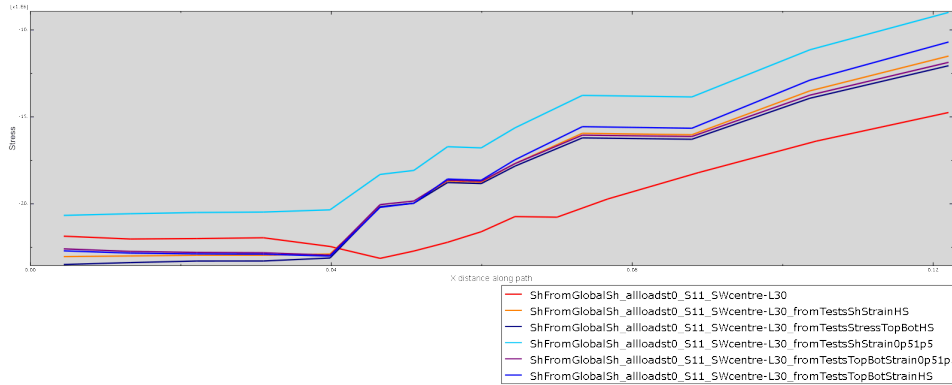


(d) Legend

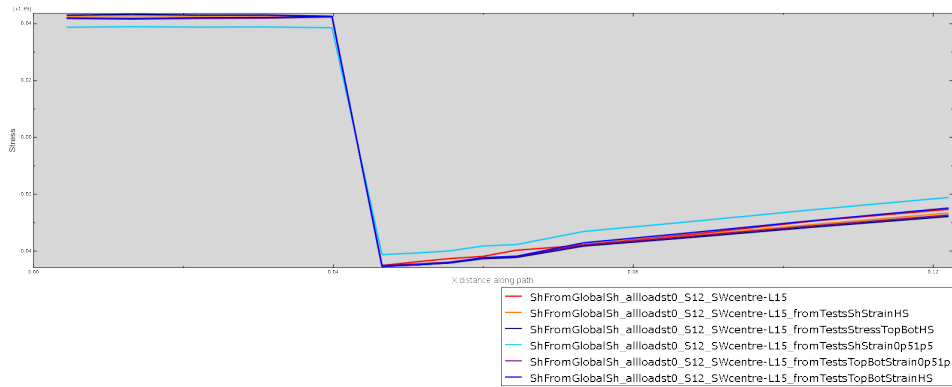
Figure 14: Blade section test cases stress results for the outer skin



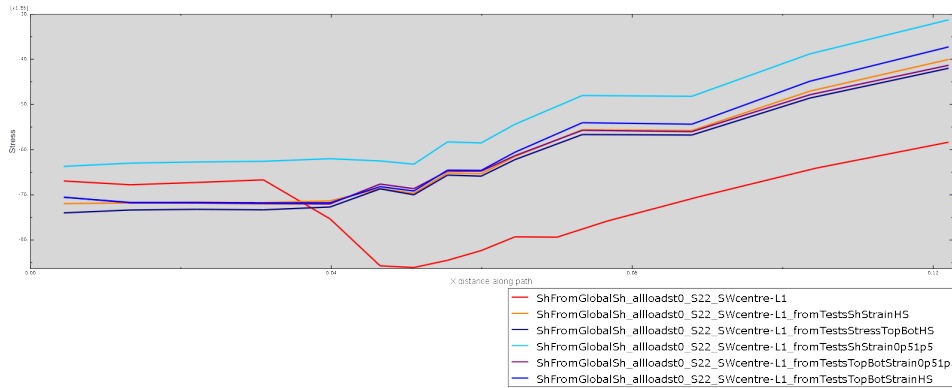
(a) S11, Shear Web Bottom of ply-1 (on the surface of the SW)



(b) S11, Shear Web last section point of ply-15 (-45, in contact with OS ply)

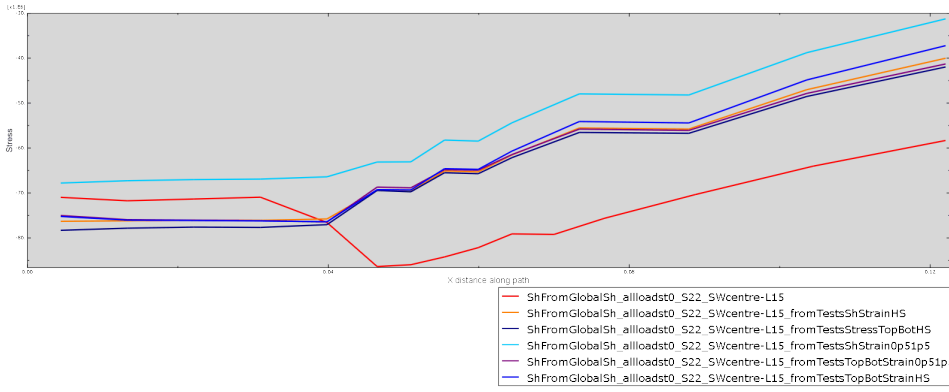


(c) S12, Shear Web ply-5

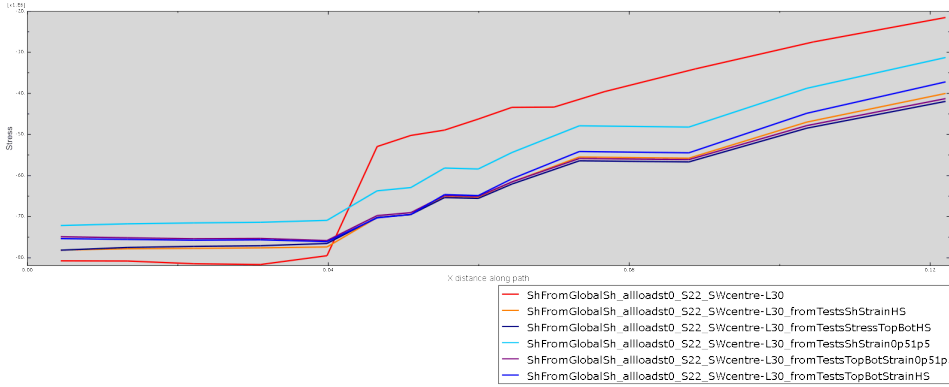


(d) S22, Shear Web Bottom of ply-1 (on the surface of the SW)

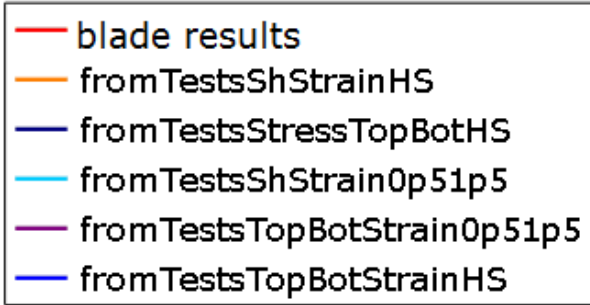
Figure 15: Blade section test cases stress results for the shear web



(a) S22, Shear Web ply-5



(b) S22, Shear Web ply-10



(c) Legend

Figure 16: Blade section test cases stress results for the shear web

## 7 Conclusions

A method to calculate detailed stresses at the T-joints of blades has been presented. The method is very dependent on the test cases used (both geometry and load cases) and on the vectors of data it uses to perform the decomposition. Further developments will focus on improving the test cases, by perusing the use of both a different geometry and different combinations of boundary conditions and loading.

## References

- [1] C. Bak et al. “Design and performance of a 10MW wind turbine”. In: *Danish Wind Power Research* (2013).
- [2] T. Burton et al. *Wind Energy Handbook*. Wiley, 2001.

- [3] J. Degrieck and W. Van Paepegem. “Fatigue damage modelling of fibre-reinforced composite materials: review”. In: *Applied Mechanics Reviews* 54.4 (2001), pp. 279–300.
- [4] *DNV-RP-C203 Fatigue design of offshore steel structures*. DNV. 2011.
- [5] M.A. Eder and Bitsche R.D. “Fracture analysis of adhesive joints in wind turbine blades”. In: *Wind Energy* (2014).
- [6] H. Gulasik and D. Coker. “Delamination-debond behaviour of composite T-joints in wind turbine blades”. In: *The science of making torque from wind 2014, Journal of Physics Conference Series* 524.012043 (2014).
- [7] Amirhossein Hajdaei. “Extending the fatigue life of a T-joint in a composite wind turbine blade”. PhD thesis. Manchester University, 2013.
- [8] B. Pascual and S. Adhikari. “A reduced polynomial chaos expansion method for the stochastic finite element analysis”. In: *Sadhana - Proceedings of the Indian Academy of Engineering Sciences* 37.3 (2012), pp. 5–17.
- [9] S.K. Sachdeva, P.B. Nair, and Keane A.J. “Comparative study of projection schemes for stochastic finite element analysis”. In: *Computer methods in applied mechanics and engineering* 195 (2006), pp. 2371–2392.
- [10] Y.Wang et al. “Finite element analysis of composite T-joints used in wind turbine blades”. In: *Plastics, Rubber and Composites* 44.3 (2016), pp. 87–97.